STUDIUL ÎMBINĂRILOR ADEZIVE DINTRE ELEMENTE COMPOZITE PULTRUDATE PRIN METODE ANALITICE ȘI NUMERICE
ANALYTICAL AND NUMERICAL STUDY OF ADHESIVELY BONDED COMPOSITE PULTRUDED ELEMENTS

DRAGOȘ UNGUREANU, NICOLAE ȚĂRANU * , DORINA NICOLINA ISOPESCU, VLAD LUPĂȘTEANU, PETRU MIHAI, IULIANA HUDIȘTEANU

Universitatea Tehnică "Gheorghe Asachi" din Iaşi, Blvd. Mangeron 43, Iaşi, Romania, 700050.

This paper presents the outcomes of a comparative study between two fibre reinforced polymer (FRP) composites adhesively bonded joints, namely the single lap joint (SLJ) and the thick adherents joint (TAJ). Thus, 18 distinct models have been conceived and analysed. The variable parameters which are considered in this study are: the bond length and the thickness of the adhesive.

The two general types of joints have been modelled in Ansys Workbench finite element analysis software. Each model has been loaded longitudinally with a tensile force of 1000 N. The parameters that characterise the surface of the FRP composite elements have been determined based on microscopic studies, through graphic and numerical processing of the images.

Based on the outcomes numerical analysis, the variation of the stresses along the bond length has been graphically illustrated. The results delivered by the numerical analysis have been compared with the ones obtained analytically, by applying the available theoretical models. It was concluded that the two methods, provide similar predictions regarding the distribution and the peak values of the shear stresses.

Această lucrare prezintă rezultatele unui studiu comparativ între două tipuri de îmbinări adezive utilizate la asamblarea elementelor compozite polimerice armate cu fibre (CPAF), și anume, îmbinarea realizată prin suprapunere simplă și îmbinarea cu aderenți rigizi. În acest sens, au fost concepute și analizate 18 modele geometrice. Parametrii variabili care au fost considerați în acest studiu sunt lungimea de conlucrare și grosimea stratului de adeziv.

Cele două tipologii de îmbinări au fost modelate cu ajutorul programului bazat pe calcul cu element finit Ansys Workbench. Fiecare model a fost încărcat cu o forță longitudinală de tracțiune, cu valoarea de 1000N. Parametrii care caracterizează suprafața elementelor CPAF au fost determinați în urma studiului microscopic, prin procesarea grafică și numerică a imaginilor captate.

Pe baza modelărilor numerice s-a trasat grafic variația tensiunilor în lungul zonei de îmbinare. Rezultatele analizelor numerice au fost comparate cu cele obținute pe cale analitică, pe baza modelelor teoretice existente. În urma studiului s-a concluzionat că ambele metode de analiză, atât numerică cât și analitică, oferă predicții similare privind distribuția și valorile ultime ale tensiunilor tangențiale.

Keywords: *adhesive joint, glass fibre reinforced polymer composite, finite element modelling, analytical models*

1. Introduction

Nowadays, the fibre reinforced polymer (FRP) composite products are widely used in various engineering applications offering significant advantages when compared to the traditional materials, in terms of low weight, corrosion resistance, high mechanical strengths and formability [1-4]. In the structural applications of FRP composite elements, the most common types of connections consist in mechanical fastening and adhesive bonding [5, 6].

Usually, the mechanical fastening connections are easily assembled, in terms of manufacturing and inspection, and can be dismantled when the structural system ends its service life. However, when connections such as riveting, pining or bolting are used to join FRP composite elements, the reinforcing fibres are cut when the fasteners' holes are executed. Thus, the discontinuities in the internal reinforcing fibres lead to significant stress concentrations and can severely decrease the load-carrying capacity of the assembly. Therefore, the adhesively bonded connections are more suitable to the anisotropic behavior of FRP composites, enabling a smoother and more uniform stress transmission through the constituents [7, 8].

The stress-strain analysis of the adhesively bonded FRP composite elements is one of the most important stages in the design of such a connection. The geometrical characteristics of the bond and the particularities of the interfaces can lead to several difficulties and uncertainties in an

* Autor corespondent/*Corresponding author*,
E-mail: taranu@ce.tuiasi.ro

accurate evaluation of the stresses and the strains along the bond length. The response of the adhesively bonded joints can be predicted by applying either analytical or numerical approaches.

The available analytical models give reliable prediction only for specific bonded joints, with particular geometrical configuration and which fail under certain criteria. Moreover, each of the available analytical models predicts only one stress component and, from this reason, if both shear and normal stresses have to be evaluated, several theoretical models are applied. For example, in case of a single lap shear joint (SLJ), by applying the Volkersen analytical model [9] only the maximum shear stresses along the bond length can be predicted. Thus, if the maximum through-thickness normal stresses have to be evaluated, the Goland and Reissner analytical model [10] should be used.

The first part of this paper presents some of the available analytical models and numerical approaches that can be used to predict the structural response of adhesively bonded composite elements. The second part presents a case study, consisting in two types of bond configurations, for which the variation and the maximum values of the shear stresses along the bond length have been evaluated based on both analytical and numerical approaches.

2. Analytical approaches

The design steps of an adhesive bond between FRP composite elements are similar to the ones which have been already proposed for bonds between traditional materials (i.e. steel-steel / steel – FRP / concrete – FRP). The most important stage of the design process consists in evaluating the maximum stresses and strains, produced by the exterior loading forces, and comparing them to the maximum corresponding values [11-13]. However, in some particular cases the structural response of adhesively bonded FRP elements might be more complex than the one specific to the adhesively bonded traditional materials. The FRP composite materials are usually macroscopically inhomogeneous and anisotropic due to the orientation of the fibres and viscoelastic due to the matrix properties [14-16].

Several authors have studied the structural response of the adhesively bonded FRP connections based on analytical approaches [17-19]. The first analyses that have been postulated were one-dimensional and the solutions were generated in terms of explicit functions for different stress components. The initial theoretical analysis for the stress distribution through an adhesive layer is accredited to Volkersen [20-22]. The Volkersen model is generally referred as “the shear lag model” and it investigates the shear deformation in the adhesive layer for the single lap joint (SLJ) made of two metal adherents. Several parameters were then assessed to the initial model in order to adapt it for the stress-strain analysis of adhesively bonded FRP composite elements.

Goland and Reissner [23-25] were the first authors that proposed a model that accounts for the additional bending moment due to the axial force applied to a bonded joint, in case of SLJ configurations. For the Goland and Reissner analytical model, the adherents are assumed to be identical and isotropic. The analysis is based on the classical theory for the infinitesimal bending of a thin elastic beam and consists in two main steps. Firstly, the overlap area is isolated and the boundary conditions for shear, bending and tension resultants are applied to characterize the influence of the connecting adherents. Secondly, the limitations due to the displacement compatibility between the adhesive and the adherents are added to the initial equations for the boundary conditions. The Goland and Reissner theoretical model may be used to investigate the distribution of the shear and the peeling stresses along the bond length, for two different types of bonded joints. The first one consists in joints made up of low modulus adherents (*i.e*. timber elements) bonded in thin and stiff adhesive layers while the second can be used when FRP composite elements are bonded to metal surfaces. Also, the second model has been derived and applied to FRP-to-FRP bonded joints.

Based on the Goland and Reissner theory, Hart-Smith [13, 26-28] proposed a new theoretical model that accounts for various types of adherents. The model assumes that the failure of a bonded joint occurs when the adhesive reaches its ultimate shear strain. The theory allows for large deformations at the adhesive level and relates the adhesive shear structural response to one of the three proposed stress-strain curve patterns [29].

Other models [30, 31] can be used to determine the stress variation through the thickness of the adhesive layer. However, these models involve extended mathematical calculation and, therefore, they are not convenient in the common design practice.

Most of the analytical models were developed for the structural analysis of the single and double lap joints, and cannot be applied to complex bond configurations. The closed-form solutions are generated considering the mechanical characteristics of the adhesive and a corresponding cohesive failure. For FRP composites adhesively bonded joints, the failure may occur at different levels (interfaces, adhesive, adherents), being influenced by several parameters (surface preparation, curing conditions, adherents’ roughness, adherents surface energy, etc.), which cannot be characterized through the analytical approaches

3. Finite element analysis (FEA)

The main advantages of using analysis based on numerical methods, consists in the possibility of obtaining the structural response for any type of bond configurations, in terms of material properties and bond geometries [32-34].

The FEA of adhesively bonded joints may be divided in three main stages, [13]: input data, finite element modeling (FEM) and output data. In the first stage, the materials physical and mechanical characteristics are defined, the 3D model is conceived and the load parameters are assigned. An important contribution that FEA approach introduces in the investigation of FRP adhesively bonded joints is the opportunity to take account of experimental data obtained through the uniaxial and the biaxial testing of the bond constitutive materials. The mechanical properties, previously obtained by experimental means, are introduced as input data.

The second stage consists in meshing of the 3D model. The FEA is based on the theory of stationary potential energy which states that the deformed shape of a loaded structure is the shape for which the stationary energy of the system is minimal [35]. The total deformation is computed considering the displacements of the nodes which are located on the model boundaries. The number of nodes and the type and the size of the mesh elements should be compatible. In the last stage, the results data are obtained and analyzed.

Others considerable contributions of the FE method to the analysis of the FRP composite adhesively bonded joints includes the possibility of selecting the failure criteria and modelling the damage propagation. These features enable the modelling of the complete structural response of an adhesive joint up to the failure point. However, the FE methods involves several drawbacks, including the convergence issues when non-linear materials and complex geometries are used [36].

4. Case study

In order to investigate the precision of different stress analysis techniques, a comparison between analytical and numerical approaches in terms of shear stress predictions is presented in this section. The configurations proposed for this comparative analysis include a SLJ and a thick adherents' joint (TAJ), both consisting in pultruded glass fibre reinforced polymer (GFRP) Fiberline profiles bonded with structural epoxy adhesive Sikadur30. The Fiberline GFRP composite profiles are made of E-glass fibres embedded in an isophthalic polyester resin. The fibres distributions consist mainly in unidirectional rovings' towards the center and two combined mats towards the outside. The combined mats are made of woven mats 0°/90° as well as chopped strand mats, both stitched together [37, 38]. The main directions for strength and stiffness of the GFRP composite profiles are presented in Figure 1. The main/longitudinal direction is indicated as 0° and the transverse direction is indicated as 90°. The properties of the constitutive materials of the considered joints are given in Tables 1 to 4.

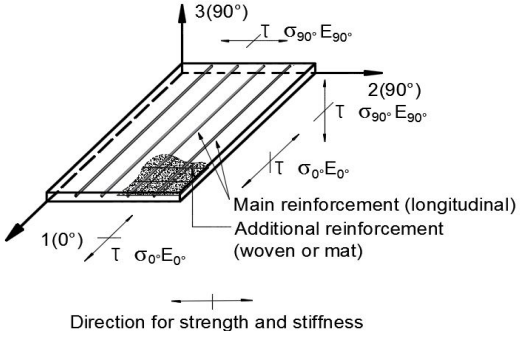

Fig. 1 - Mechanical properties of Fiberline composite strips with respect to principal directions / *Proprietățile mecanice ale platbenzilor compozite Fiberline, după direcțiile principale.*

Table 1

Properties of the adhesive [39]/ *Proprietățile adezivului*

Name / *Denumire*	Density / *Densitate* [kg/m^3]	Compressive strength / *Rezistența la compresiune* $f_{c,a}$ [MPa]	Tensile strength / *Rezistența la întindere* $f_{t,a}$ [MPa]	Modulus of elasticity / *Modulul de elasticitate* E_a [GPa]
Sikadur 30	1650	70-80	24-27	11.2

Table 2

Fiberline GFRP composite strip. Physical characteristics [40]/ *Fiberline platbenzi CPAF de sticlă. Proprietățile fizice*

Density / *Densitate* [kg/m^3]	Operating temperature / *Temperatură de lucru* [ºC]	Fibre volume fraction / *Fracțiunea volumetrică de fibră* [%]
1500	-20 ~ +80	>60

Table 3

Fiberline composite strips. Elasticity moduli and Poisson's ratios [40]/ *Platbenzi compozite Fiberline. Modulii de elasticitate și coeficienții lui Poisson*

Longitudinal elasticity modulus / *Modulul de elasticitate longitudinal* [GPa]	Transversal elasticity modulus / *Modulul de elasticitate transversal* [GPa]	Modulus in shear / *Modulul de elasticitate la forfecare* [GPa]	Poisson's ratio, 0^0, 90^0 / *Coeficientul lui Poisson* 0^0, 90^0	Poisson's ratio, 90^0, 0^0 / *Coeficientul lui Poisson* 90^0, 0^0
23	8.5	3	0.23	0.09

Table 4

Fiberline composite strips. Characteristics strengths [40]/ *Platbenzi compozite Fiberline. Rezistențe caracteristice*

Tensile strength, 0^0 / *Rezistența la întindere, 0^0* [MPa]	Tensile strength, 90^0 / *Rezistența la întindere, 90^0* [MPa]	Compressive strength, 0^0 / *Rezistența la compresiune, 0^0* [MPa]	Compressive strength, 90^0 / *Rezistența la compresiune, 90^0* [MPa]
240	50	240	70

Table 5

Geometrical characteristics of the models / *Caracteristicile geometrice ale modelelor*

Model / *Model*	Type / *Tip*	Bond length / *Lungimea de conlucrare* [mm]	Adhesive layer thickness / *Grosimea stratului de adeziv* [mm]
S1-1(2, 3)	SLJ	70	1, 2, 3
S2-1(2, 3)	SLJ	100	1, 2, 3
S3-1(2, 3)	SLJ	150	1, 2, 3
T1-1(2, 3)	SLJ	70	1, 2, 3
T2-1(2, 3)	SLJ	100	1, 2, 3
T3-1(2, 3)	SLJ	150	1, 2, 3

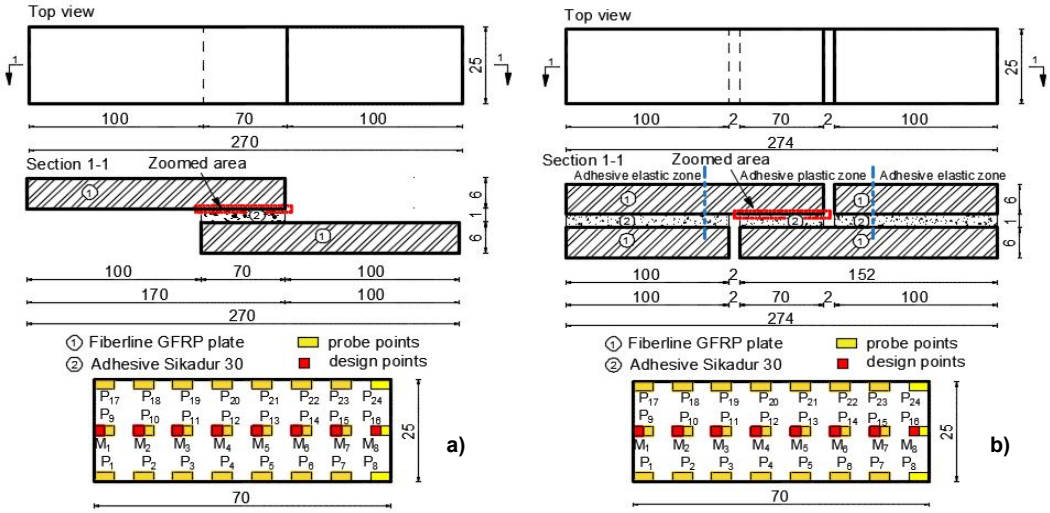

Fig. 2. a) SLJ and b) TAJ model - geometries in mm (not at scale) / *a) modelul SLJ și b) modelul TAJ – caracteristici geometrice; dimensiuni în mm (figurile nu respectă scara)*

5. Model geometry

The geometry of a bonded joint plays an important role on the structural behaviour in both analytical and numerical analyses [34]. Thus, a wide range of combinations between the bond length (70 mm, 100 mm, 150 mm) and the adhesive thickness (1 mm, 2 mm, 3 mm) have been selected for this study. In order to be easily identified and appealed to, when the results will be analysed and compared, each specimen was marked with a nominal code (Table 5). For the numerical models, specific points were considered at the interface layer between the GFRP composite and the adhesive. These points are generally referred to as probe measuring points and are used to closely record the stress variation in a specific region of the specimen. For this study, three series of probe measuring points were considered, two series located at the free edges of the bond area and one series located at the middle line of the overlap region (Fig. 2.).

The proposed configurations, the nominal dimensions of the specimens and the location of the probe measuring points for the S1-1 and T1-1 models (Table 4) are presented in Figure 2.

For all the models, the distance between two consecutive probe measuring points was kept constant at 10 mm. Thus, 24 probe points have been used for S1-1(2, 3); T1-1(2, 3) models, 33 probe points have been used for S2-1(2, 3); T2-1(2, 3) models and 48 probe points have been used for S3-1(2, 3); T3-1(2, 3) models.

6. Analytical approach

The closed form solutions for the SLJ specimens have been obtained applying an analytical model based on Goland and Reissner theory [13, 23-25] while the TAJ specimens where

investigated through the analytical model developed for joints made up according to D3165 norm [41, 42].

The analytical model of the SLJ [13, 23-25] accounts for the additional bending moment due to the axial force applied to a bonded joint. For this model, the maximum shear stress is computed using Eq. (1):

$$\zeta_0^{ultim} \approx \frac{\sigma}{8}(1+3k)\sqrt{8\frac{G_a t}{Et_a}} \qquad [1]$$

Where:

$$\sigma = \frac{P_k d\gamma_f}{t};$$

$$k = \frac{\cosh(u_2 c)\sinh(u_1 L)}{\sinh(u_1 L)\cosh(u_2 c) + 2\sqrt{2}\cosh(u_1 L)\sinh(u_2 c)};$$

$$u_1 = 2\sqrt{2}u_2; \qquad u_2 = \frac{1}{\sqrt{2}t}\sqrt{3(1-\nu^2)\frac{\sigma}{E}};$$

and

P_k – tensile force per unit length [N/m]; υ – Poisson's coefficient of the adhesive; G_a – shear modulus of elasticity of the adhesive [MPa]; E – modulus of elasticity of the adherents [MPa]; $c = \frac{L}{2}$ [mm]; L – overlap length [mm]; t_a – thickness of the adhesive layer [mm]; t – thickness of the adherents [mm]; γ_f – ultimate strain of the adhesive.

For the analytical model based on ASTM D3165 provisions, the adherents were assumed to be linear elastic and the adhesive was assumed to be elastic-perfectly plastic following von Mises yield criterion [42]. The specimens have been divided into three regions: a plastic zone located at the overlap area, within which the adhesive shear stress reach its yield strength and two adjacent elastic zones located outside the overlap area. The adhesive structural behaviour in the plastic zone is as follows:

$$\sigma_x \approx \frac{E}{(1+\upsilon)(1-\upsilon)}\left[(1-\upsilon)\varepsilon_x + \varepsilon_z\right];$$

$$\sigma_y \approx \frac{\upsilon E}{(1+\upsilon)(1-2\upsilon)}\left(\varepsilon_x + \varepsilon_z\right);$$

$$\sigma_z \approx \frac{E}{(1+\upsilon)(1-2\upsilon)}\left[\upsilon\varepsilon_x + (1-\upsilon)\varepsilon_z\right];$$

$$\zeta_{xz} = \zeta_p \approx \frac{\sigma_{yield}}{\sqrt{3}};$$

Where:

E – modulus of elasticity of the adhesive [MPa]; υ – Poisson's coefficient for the adhesive; σ – adhesive stress [MPa]; σ_{yield} – yielding strength of the adhesive [MPa]; ε – adhesive strain [mm/mm].

7. Numerical modelling

The specimens have been numerically modelled using ANSYS Workbench software [43]. The numerical models of the SLJs consists in three primitives of parallelepiped shapes, while for the TAJs models seven primitives were used. The primitives' forms have been connected together to match the geometric configurations. A primitive of parallelepiped shape is defined by eight nodes, each node having three degrees of freedom. For each node, the parameters of position and connectivity have been defined.

The final models have been meshed using rectangular elements of 0.2 to 1 mm in length for the adhesive layer and 2 mm for the adherents. The discretization procedures are depicted in Fig. 3a. The loading conditions are presented in Fig. 3b.

A refined mesh has been used for the overlap area. The refinement level has been set to 0.1, meaning that the maximum length of the triangular/rectangular element of mesh is equal to 0.1 mm. For the mesh refinement, a smooth transition region has been considered around the probe measuring points and near the bond ends. Using a smooth mesh and a corresponding refinement level, it is ensured that any variation in stresses at the adhesive-adherent interfaces will be recorded. The GFRP strips have been modelled as being linear elastic orthotropic materials, while the adhesive was modelled as a linear elastic isotropic material.

The bond strength at the interface level is influenced by the type of the interfacial connection and by the adhesion mechanisms [42, 44, 45]. For this study, the interface surfaces between the GFRP composite elements and the adhesive have been modelled according to the mechanical theory of adhesion. Based on this theory, the degree of adhesion that can be obtained for a bonded joint is

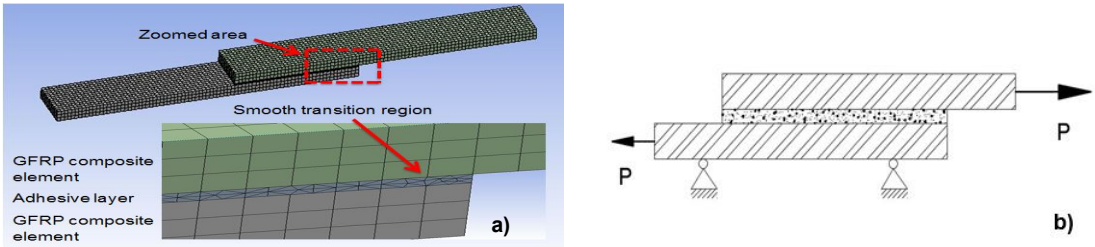

Fig. 3. a) Meshing of the 3D model; b) Loading conditions / *a) Discretizarea modelului tridimensional; b) Condiții de încărcare* .

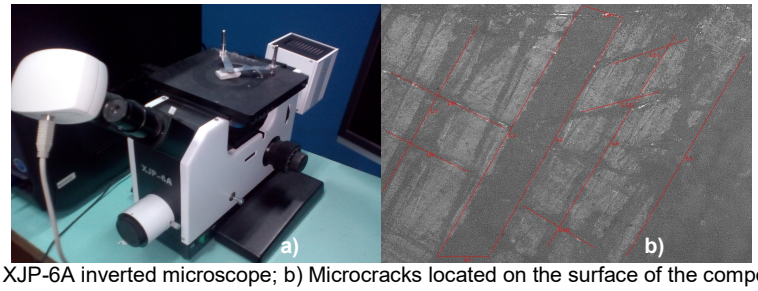

Fig. 4. a) XJP-6A inverted microscope; b) Microcracks located on the surface of the composite strip / *a) Microscop inversat XJP-6A; b) Microfisuri la suprafața platbenzii compozite*

Table 5

Dimensions of the microcracks/ *Dimensiunile microfisurilor*

Microcracks / *Microfisuri*	L1	L2	L3	L4	L5	L6	L7	L8	L9
Dimensions / *Dimensiuni* [μm]	1726.01	1594.94	289.47	240.51	1401.48	1481.25	1139.62	727.42	527.4

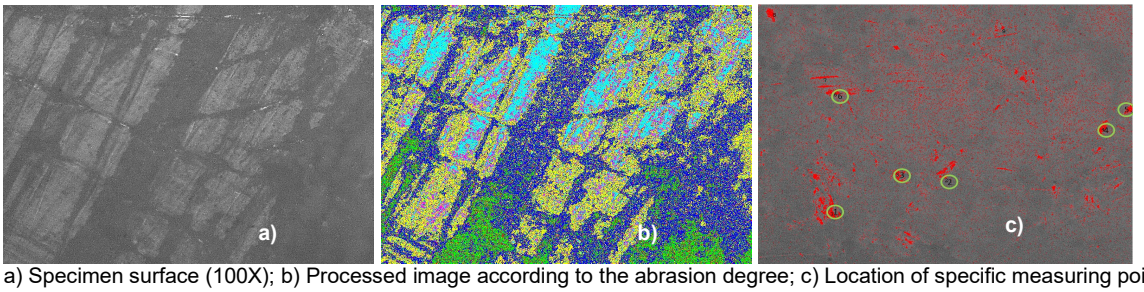

Fig. 5. a) Specimen surface (100X); b) Processed image according to the abrasion degree; c) Location of specific measuring points/ *a) Suprafața probei (100X); b) Imaginea procesată corespunzător gradului de șlefuire; c) Locația punctelor de măsurare*

Table 6

Geometrical characteristics of the regions on the surface of the specimen
Caracteristicile geometrice ale regiunilor identificate pe suprafața probei

Area / Aria	A1	A2	A3	A4	A5	A6
[μm^2]	183614.958	433220.222	1072465.374	952603.878	265207.756	416987.535
[%]	5.524	13.033	32.263	28.657	7.978	12.544

directly linked to the porosity and to the surface roughness of the substrates. The porosity of the GFRP composite elements and the average diameter of the surface particles were analysed using a XJP-6A inverted microscope equipped with a DV-2C camera (Fig. 4a). The images captured with this device were examined using the Material Plus Image Software. For determining the surface properties of the FRP composite element, a 30x30 mm specimen has been prepared. The specimen was cleaned by solvent whipping and mechanically abraded with a wire wheel brush. The over abraded regions of the specimen surface are characterised by the number and the dimensions of the microcracks. Since the latter is of relative small dimensions (max 1.7mm) (Fig. 4b, Table 5), this surface preparation technique may be considered to be non-invasive.

The image captured by the microscope camera (Fig. 5a) was examined using a light filter. Based on the intensity/grey scale, 6 regions were identified on the specimen surface, each region corresponding to a different degree of abrasion. The over abraded regions are represented by concentration of dark spots, while the light abraded regions appear as concentration of light spots (Fig. 5a). For better understanding, the image was processed and different colours were assessed to each region (Fig. 5b).

As it is depicted in Figure 5b, a smooth transition is observed from one region to another. Since the difference between two consecutive areas is smaller than 20% from the total area (Table 6), (area 1 and area 5 are not taken into account, because they represent less than 8% from the total area), a single value for the pure penalty coefficient of the adhesive was selected in the numerical analysis. In some particular cases, the surface of the element may be characterized by significant differences in the characteristic areas. This is valid for elements with highly irregular topographic profile. Therefore, several penalty coefficients are used in the numerical analysis.

Based on the processed image (Fig. 5b), it was found that the most suitable plane geometry of the surface cavities is the circle. Furthermore, comparing the image captured by the microscopes camera (Fig. 5a) with the processed image (Fig. 5b) an approximately metric scale was assessed for the computation of the deepness of the cavities. A specific measuring point was assessed to the centroid of each characteristic region located on the surface of the specimen. The

Table 7

Particle dimensions / *Dimensiunile particulelor*

Point / *Punctul*	1	2	3	4	5	6
Roundness / *Circularitate*	55.839	48.5	38.675	37.3	50.538	43.069
Aspect ratio / *Raport dimensional*	1	1.867	1	1	1.494	1
Circle diameter [μm] / *Diametrul cercului [μm]*	121.160	58.506	94.113	114.727	81.450	95.969
Sphere volume [μm]^3 / *Volumul sferei [μm]^3*	134406.517	15133.450	62992.78	114115.214	40833.542	66794.562

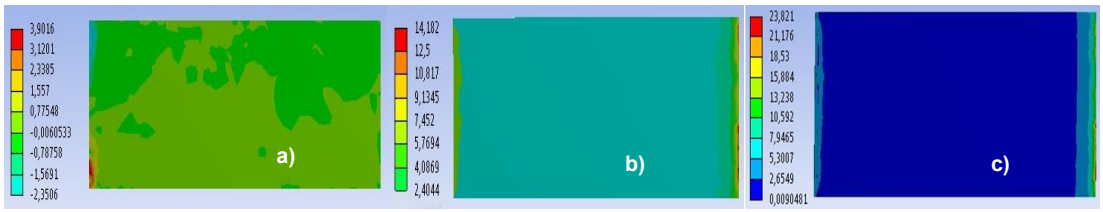

Fig. 6 - Adhesive a) shear stress distribution; b) peel stress distribution; c) von Mises stress distribution; for S1-1 model [MPa]*/ Harta distribuției tensiunilor a) tangențiale; b) de cojire, c) von Mises în stratul de adeziv pentru modelul S1-1 [MPa]*

roundness of the surface particles located centremost to the monitoring points was measured and small differences from the spherical geometry were observed (0.018539 mm deviation in diameter and height). The measurements of the height of the surface particles and of the depth of the surface cavities were performed according to the intensity grey scale.

Since the roundness and circularities deviations are insignificant, the average diameter of the particles was selected as value for the penetration coefficient. The latter is utilised in the numerical analysis and it indicates the level in mm for which the adhesive penetrates the adherent surface. The location of the specific measuring points is indicated in Fig. 5c and the measuring data are given in Table 7. The red coloured zones correspond to the over abraded regions, and therefore are not suitable for particle measurements. Since the initial location of the measuring points 5 and 6 coincided with an over abraded area, the points were permuted to the close vicinity.

Based on the results obtained from the microscopic analysis of the specimen, the contact region between the adhesive and the GFRP composite element was modelled as a *bond contact* with *pure penalty formulation*. The contact detection was set to the nodal points where the normal axis is perpendicular to the plane of the contact surface. The penetration factor was selected as the average value computed for the surface particles diameters (0.0943 mm, Table 6).

8. Results

The FEA of the SLJ and the TAJ models showed that the adhesive layers are predominantly loaded in shear. However, significant concentrations of peel stresses located at the overlaps ends can be observed for the SLJ models corresponding to S1 series (models with bond length of 70 mm), (Fig. 6b). For the TAJ and SLJ models with bond lengths of 100 mm and 150 mm, the influence of the peeling stresses concentrations on the final structural response of the bond is neglectable. Therefore, only the shear stress variation was graphically depicted and analysed in this paper.

For each set of three transverse, consecutive probe measuring points, the average value of the shear stresses was computed. Thus, 8 design values for the models S1-1(2, 3); T1-1(2, 3), 11 design values for the models S2-1(2, 3); T2-1(2, 3) and 16 design values for the models S3-1(2, 3); T3-1(2, 3) were obtained.

Using the values computed for the specific points (M1, M2,…,M16), (Fig. 6), the distributions of the shear stresses within the overlap area were graphically represented (Figs. 7-10; 13-15). The shear stresses along the bond length have been also evaluated based on the existing analytical models and the corresponding values have been compared to the ones obtained through the numerical analyses.

The shear stress, the peeling stress and the von Misses stress maps for the S1-1 model (isolated overlap) acted by a tensile force of 1000 N are displayed in Fig.6. The graphical representations of the shear stress distribution computed through both analytical and numerical approaches are presented in Fig. 7a, b.

The results obtained through the numerical and the analytical approaches are in good agreement. The shear stress distribution patterns are similar for both the SLJ and TAJ models. The maximum values of the shear stresses that were obtained applying the numerical method are slightly greater than the ones predicted by the analytical models. The distribution of the shear stresses along the bond length of the SLJ models, evaluated by both analytical and numerical approaches, is graphically presented in Figs. 8-10.

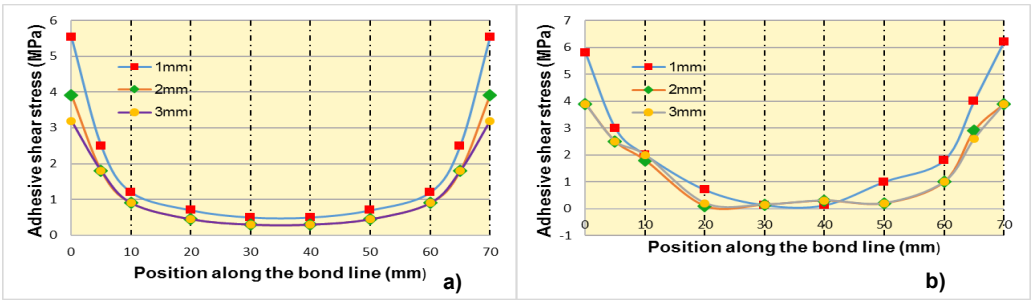

Fig. 7 - Adhesive shear stress distribution: a) from analytical model; b) from FEA [MPa]/ *Distribuția tensiunilor tangențiale în stratul de adeziv obținută: a) pe cale analitică; b) pe baza analizei numerice [MPa]*

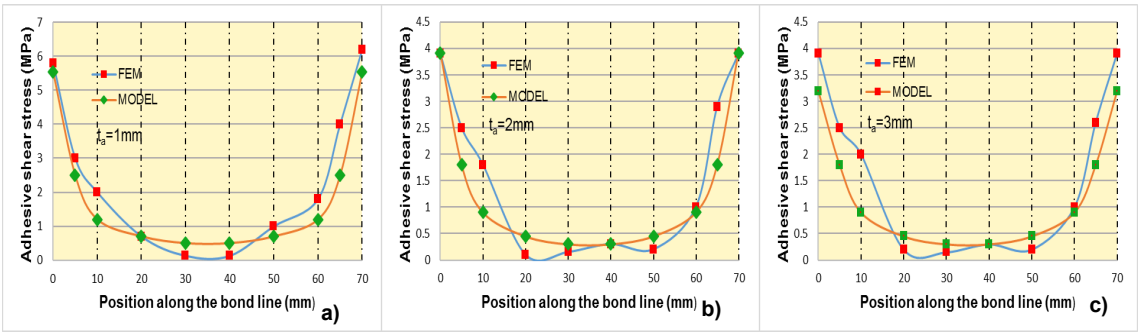

Fig. 8 - Adhesive shear stress distribution for: a) S1-1; b) S1-2; c) S1-3/ *Distribuția tensiunilor tangențiale în stratul de adeziv pentru: a) S1-1; b) S1-2; c) S1-3*

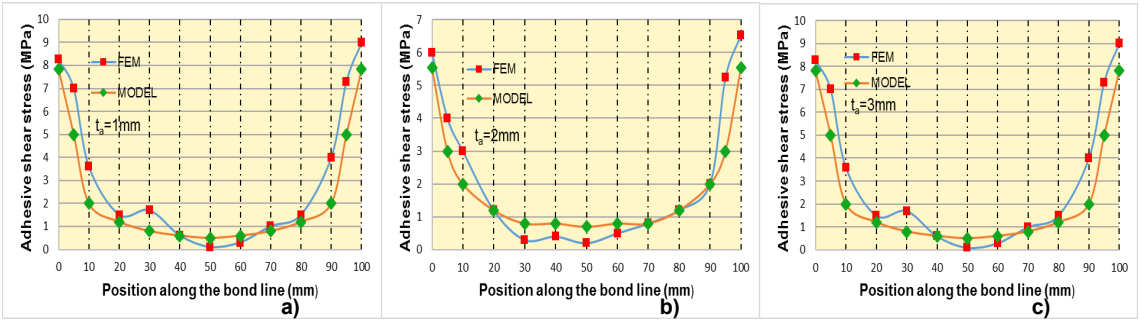

Fig. 9 - Adhesive shear stress distribution for: a) S2-1; b) S2-2; c) S2-3/ *Distribuția tensiunilor tangențiale în stratul de adeziv pentru: a) S2-1; b) S2-2; c) S2-3*

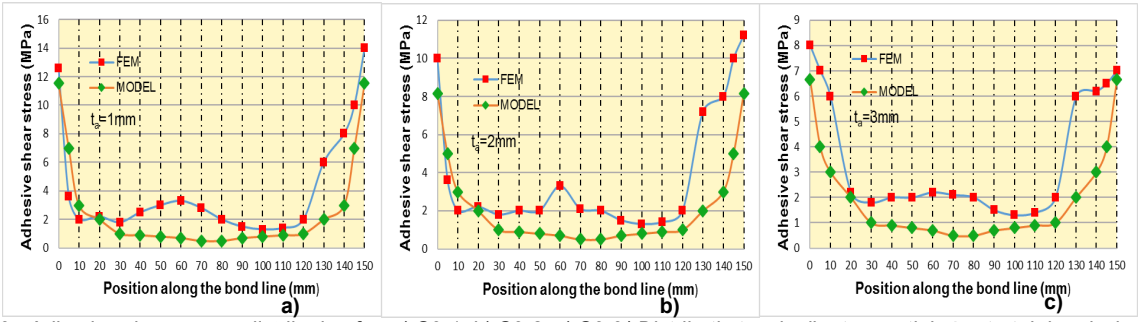

Fig. 10 - Adhesive shear stress distribution for: a) S3-1; b) S3-2; c) S3-3/ *Distribuția tensiunilor tangențiale în stratul de adeziv pentru: a) S3-1; b) S3-2; c) S3-3*

The peelings stress for the TAJ configuration, concentrated at the overlaps ends are smaller than the ones obtained for the SLJ configuration, even for the models with 70 mm bond lengths. The shear stress, the peeling stress and the von Misses stress maps for the T1-1 model (isolated overlap) acted by a tensile force of 1000 kN are displayed in Figure 11.

The distribution of all stress components for the TAJ T1-1 model, evaluated by both analytical and numerical approaches is presented in Figure 12. The comparison between the shear and the peeling stresses distributions evaluated through analytical and numerical methods is graphically represented in Fig. 13.

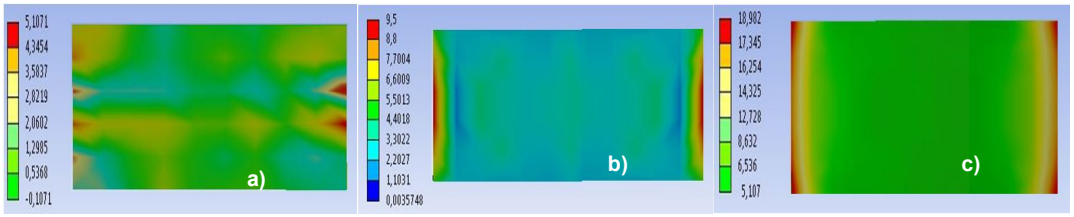

Fig. 11 - Adhesive stress maps a) shear stress; b) peel stress c) von Misses stress for TAJ model T1-1 [MPa]/ *Harta tensiunilor în stratul de adeziv a) tangențiale; b) de cojire c) von Misses pentru îmbinarea cu aderenți rigizi T1-1 [MPa]*

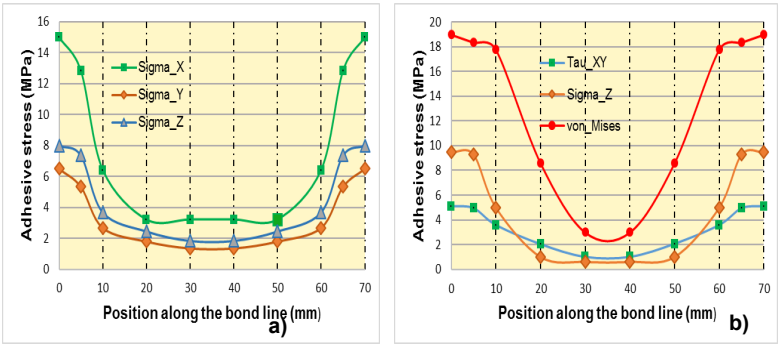

Fig. 12 - Adhesive stress distributions from: a) analytical model; b) numerical analysis (ANSYS), for the TAJ specimen T1-1/ *Distribuția tensiunilor în stratul de adeziv pentru modelul T1-1 obținută: a) pe cale analitică; b) pe baza analizei numerice [MPa]*

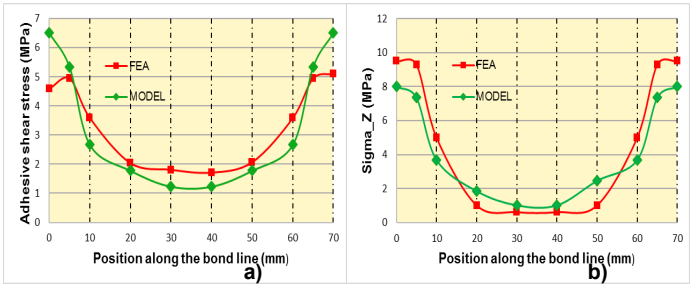

Fig. 13 - Comparison between analytical and numerical results - Stress distribution along the bond line for TAJ model T1-1 a) shear stress; b) peeling stress / *Comparație între rezultatele analitice și cele numerice - Distribuția tensiunilor în lungul zonei de îmbinare pentru modelul TAJ T1-1 a) tensiuni tangențiale; b) tensiuni de cojire*

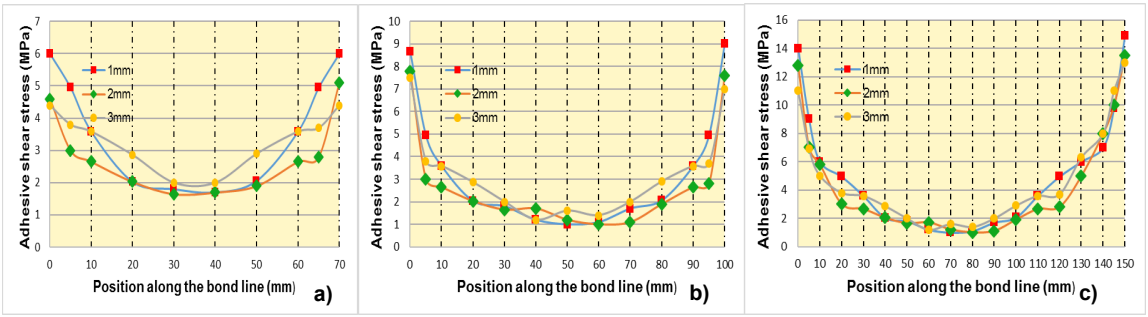

Fig. 14 - Adhesive shear stress distribution from numerical analysis (ANSYS): a) T1-1(2, 3); b) T2-1(2,3); c) T3-1(2, 3) / *Distribuția tensiunilor tangențiale în adeziv conform analizei numerice (ANSYS): a) T1-1(2, 3); b) T2-1(2,3); c) T3-1(2, 3)*

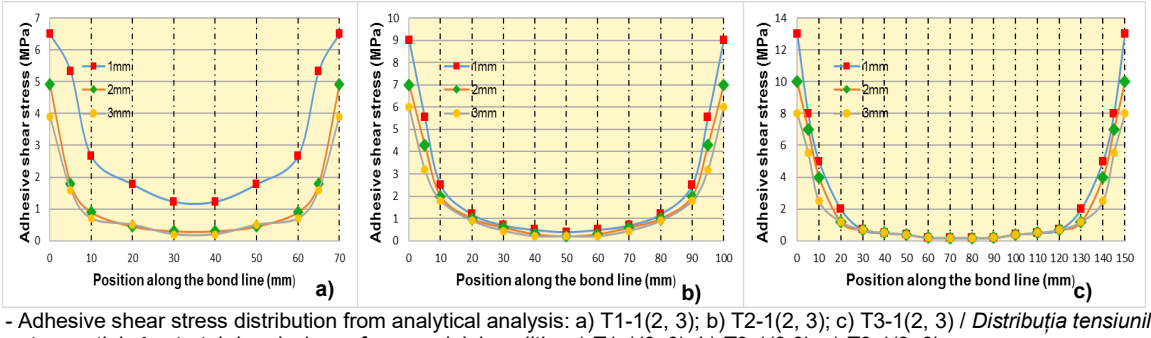

Fig. 15 - Adhesive shear stress distribution from analytical analysis: a) T1-1(2, 3); b) T2-1(2, 3); c) T3-1(2, 3) / *Distribuția tensiunilor tangențiale în stratul de adeziv conform modelul analitic: a) T1-1(2, 3); b) T2-1(2,3); c) T3-1(2, 3)*

The distribution of the shear stresses along the bond length of the TAJ models, evaluated by both numerical and analytical approaches, are graphically presented in Figs. 14, 15.

4. Conclusions

This paper presents the essential features related to the structural response of adhesively bonded FRP composite pultruded elements. Based on the results that have been obtained by applying both theoretical and numerical approaches, the following conclusions can be drawn:

1. The analytical models proposed for bonds between FRP composite elements give reliable predictions only for specific bonded joints, with particular geometrical configuration and which fail under certain criteria. For complex bond configurations, in terms of material properties and bond geometry, the complete structural response up to the failure point can be obtained by applying numerical analysis based on the finite element method.

2. For the two types of bond configurations, SLJ and TAJ, a generally good agreement has been observed for the results obtained through the analytical and the numerical approaches. The structural analysis of the models showed that the adhesive layers are predominantly loaded in shear. However, significant peel stress concentrations tend to be formed near the overlap ends for the SLJ models with 70 mm bond length.

3. For both type of specimens, the ultimate values of the shear stresses obtained by numerical approach are slightly greater than the ones obtained by applying the analytical models (max 32% for S3-2 model). The analytical model developed for joints made up according to D3165 norm give closer predictions to the numerical analysis results in terms of maximum shear and peeling stress. Furthermore, the analytical model based on D3165 provisions, can be used to investigate the complete structural response of the TAJs composed of FRP elements.

4. Unlike the analytical methods, the numerical analysis techniques account for several auxiliary parameters, such as: irregular boundaries, different materials, variable elements size and nonlinear problems.

REFERENCES

1. N. Țăranu, C. Banu, G. Oprișan, M. Budescu, V. Munteanu, O. Ioniță, Tensile characteristics of glass fibre reinforced polymeric bars, Romanian Journal of Materials, 2010, **40**(4), 323.
2. V. Lupășteanu, N. Țăranu, P. Mihai, G. Oprișan, R. Lupășteanu, D. Ungureanu, Behaviour of CFRP-to-steel interfaces in adhesively bonded joints, Romanian Journal of Materials, 2016, **46**(4), 515.
3. L. Bejan, N. Țăranu, A. Sârbu, Advanced polymeric composites with hybrid reinforcement, Journal of optoelectronics and advanced materials, 2010,**12**(9), 1930.
4. M. Dima, C. Frâncu, Methods for testing glass fibre reinforced polymer composites (GFRP'S) with polyester matrix, Rom. Jou. Mat, 2014, **44**(3), 304.
5. N. Țăranu, D. Banu, G. Oprișan, M. Budescu, L. Bejan, Strengthening of thin reinforced concrete slabs with composite strips, Rom. Jou. Mat, 2013, **43**(1), 3.
6. S. V. Nimje, S. K. Panigrahi, Interfacial failure analysis of functionally graded adhesively bonded double supported tee joints of laminated FRP composite plates, International Journal of Adhesion & Adhesives, 2015, **58**, 70.
7. D. Ungureanu, N. Țăranu, V. Lupășteanu, P. Mihai, I. Hudișteanu, Behaviour of composite-to-composite interface for adhesively bonded joints. Experimental set-up, Buletinul Institutului Politehnic din Iași, 2016, **62(66)**(3), 29.
8. A. A. Taib, R. Boukhili, S. Achiou, S. Gordon, H. Boukehili, Bonded joints with composite adherends. Part I. Effect of specimen configuration, adhesive thickness, spew fillet and adherend stiffness on fracture, International Journal of Adhesion & Adhesives, 2006, **26**(4), 226.
9. T. Vallee, T. Tannert, J. Murcia-Delso, D. J. Quinn, Influence of stress-reduction methods on the strength of adhesively bonded joints composed of orthotropic brittle adherends, International Journal of Adhesion & Adhesives, 2010, **30**(7), 583.
10. M. Goland, E. Reissner. The stresses in cemented joints, Journal of Applied Mechanics, 1944, **1**(1), 17.
11. V. M. Karbhari, Rehabilitation of Metallic Civil Infrastructure Using Fiber Reinforced Polymer (FRP) Composites, Woodhead Publishing, Texas, SUA, 2014. R. Haghani, Finite element modelling of adhesive bonds joining fibre-reinforced polymer (FRP) composites to steel.
12. T. Vallee, J. R. Correia, T. Keller, Probabilistic strength prediction for double lap joints composed of pultruded GFRP profiles – Part II: Strength prediction, Composites Science and Technology, 2016, **66**(13), 1903.
13. L. Groll, N. Țăranu, Îmbinări la elemente din materiale compozite, Editura Societății Academice "Matei – Teiu Botez", Iași, 2003.
14. L. Lilleheden, Mechanical properties of adhesives in situ and in bulk, International Journal of Adhesion & Adhesives, 1994, **14**(1), 31.
15. T. Keller, T. Vallee, Adhesively bonded lap joints from pultruded GFRP profiles. Part I: stress-strain analysis and failure modes, Composites Part B: engineering, 2005, **36**(4), 331.
16. T. Vallee, T. Tannert, R. Meena, S. Hehl, Dimensioning method for bolted, adhesively bonded, and hybrid joints involving Fibre-Reinforced-Polymers, Composite Part B: engineering, 2013, **46**, 179.
17. N. Stein, H. Mardani, W. Becker, An efficient analysis model for functionally graded adhesive single lap joints, International Journal of Adhesion & Adhesives, 2016, **70**, 117.
18. H. Abdi, J. Papadopoulos, H. Nayeb-Hashemi, A. Vaziri, Enhanced elastic-foundation analysis of balanced single lap adhesive joints, International Journal of Adhesion & Adhesives, 2016, **72**, 80.
19. N. Stein, P. Weißgraeber, W. Becker, Stress solution for functionally graded adhesive joints, International Journal of Solids and Structures, 2016, **97-98**, 300.
20. P. Cognard, Adhesives and Sealants General Knowledge, Application Techniques, New Curing Techniques, Volume 2, Elsevier Science, 2006, R. J. Moulds, Chapter 3 – Design and Stress Calculations for Bonded Joints.
21. R. Q. Rodríguez, W. P. de Paiva, P. Sollero, M. R. B. Rodrigues, É. L. de Albuquerqueb, Failure criteria for adhesively bonded joints, International Journal of Adhesion and Adhesives, 2012, **37**, 26.
22. H. Özera, Ö. Öz, Three dimensional finite element analysis of bi-adhesively bonded double lap joint, International Journal of Adhesion and Adhesives, 2012, **37**, 50.
23. Z. J. Wu, A. Romeijn, J. Wardenier, Stress expressions of single-lap adhesive joints of dissimilar adherends, Composite Structures, 1997, **38**(1), 273.
24. D.W. Oplinger, Effects of adherend deflections in single lap joints, International Journal of Solids and Structures, 1994, **31**(18), 2565.
25. Q. Luo, L. Tong, Fully-coupled nonlinear analysis of single lap adhesive joints, International Journal of Solids and Structures, 2007, **44**(7-8), 2349
26. L. J. Hart-Smith, Adhesive-bonded single-lap joints, NASA Langley Research Center, Hampton, VA, 1973, CR-112236.
27. L. J. Hart-Smith, Adhesive-bonded double-lap joints. Douglas Aircraft Company, NASA, 1973, CR-112235.
28. L. C. Hollaway, Polymers and polymer composites in construction, UK, 1990.
29. W. S. Johnson, Delamination and debonding of materials, ASTM special technical publication 876, NASA Langley Research Center, Philadelphia, 1983, L. J. Hart-Smith, Designing to minimize peel stresses in adhesive-bonded joints.
30. D. J. Allman, A theory for elastic stresses in adhesive bonded lap joints, The Quarterly Journal of Mechanics and Applied Mathematics, 1977, **30**(4), 415.
31. D. Chen, S. Cheng, An analysis of adhesive-bonded single-lap joints, Journal of Applied Mechanics, 1983, **50**(1), 109.
32. E. J. Barbero, Finite Element Analysis of composite materials using Ansys, CRC Press Taylor and Francis Group, USA, 2014.
33. D. Linghoff, Steel members strengthened with carbon fibre reinforced polymers, PhD thesis, Chalmers University of Technology, Sweden.
34. N. Țăranu, S. Popoaei, G. Oprișan, P. Ciobanu, P. Mihai, V. Munteanu, Influence of assembling parameters on joints behaviour of pultruded elements made of fibre reinforced polymer composites, Rom. Jou. Mat., 2014, **44**(3), 236.
35. G. Li, Elastic analysis of closed-form solutions for adhesive stresses in bonded single-strap butt joints, Journal of Mechanics of Materials and Structures, 2010, **5**(3), 408
36. G. Oprișan, N. Țăranu, M. Budescu, I. Ențuc, Structural behaviour of reinforced concrete beams strengthened by CFRP plate bonding, Rom. Jou. Mat., 2012, **42**(4), 387.
37. T. Vallee, T. Keller, Adhesively bonded lap joints from pultruded GFRP profiles. Part: III: Effects of chamfers, Composites Part B: engineering, 2006, **37**(4), 328.
38. T. Vallee, T. Keller, G. Fourestey, B. Fournier, J. R. Correia, Adhesively bonded joints composed of pultruded adherends: Considerations at the upper tail of the material strength statistical distribution, Probabilistic Engineering Mechanics, 2009, **24**(3), 358.
39. xxx, Sikadur 30, Product data sheet, Identification no: 02040104001000001, 2014, UK.
40. xxx, Fiberline design manual, Flat profiles, plates and sheets, 2012.
41. xxx, ASTM D3165 - 07(2014), Standard Test Method for Strength Properties of Adhesives in Shear by Tension Loading of Single-Lap-Joint Laminated Assemblies, 2014.
42. C. Yang, J. S. Tomblin, Z. Guan, Analytical modeling of ASTM lap shear adhesive specimens, U.S. Department of Transportation Federal Aviation Administration Office of Aviation Research Washington, DC 20591, DOT/FAA/AR-02/130, 2003.
43. ANSYS Workbench user's guide, Canonsburg, Pennsylvania, USA, 2009
44. N. Țăranu, R. Cozmanciuc, I. Ențuc, M. Budescu, V. Munteanu, D. Isopescu, The behaviour of the interface between carbon fibre reinforced polymer composite plates and concrete, Rom. Jou. Mat., 2015, **45**(3), 226.
45. D. Ungureanu, N. Țăranu, V. Lupășteanu, A. R. Roșu, P. Mihai, The adhesion theories applied to adhesively bonded joints of fiber reinforced polymer composite elements, Buletinul Institutului Politehnic din Iași, 2016, **62(66)**(2), 37.

1.